STUDIA Z AUTOMATYKI I INFORMATYKI
TOM 43 – 2018

Paul F. Easthope*, Alan Collinson†

# TRACKING SWARMS OF UNMANNED AERIAL SYSTEMS

**Keywords:** UAS swarms, swarm tracking, Kalman Filters

## 1. INTRODUCTION

The proliferation of cheap Unmanned Aerial Systems (UAS), also known as Unmanned Aerial Vehicles (UAVs), poses significant challenges for Ground Based Air Defence (GBAD) systems. Individual UAS are inherently difficult to detect, track, classify and identify and these challenges are exacerbated if UAS are employed in swarms.

Swarm technology and its applications are now sufficiently advanced that they have been reported in readily available open-source literature (see, for example, [12], [1]). The accessibility of this information may provide a vector for further development by adversaries and it is likely to be only a matter of time before such swarms are used with malign intent.

The emphasis of this paper is primarily upon the development of tracking algorithms able to cope with swarms of UAS, since the simulation of such potential threats has already been addressed ([12], [6]), while the tracking of such swarms represents an emerging challenge. Section 2 provides background information on existing categories of UAS and discusses in more detail why they provide a challenge for tracking systems; this background material is also beneficial from the simulation point of view. Section 3 outlines a simple UAS simulation that is sufficient to demonstrate the tracking logic described in Section 4.

## 2. UAS BACKGROUND

UAS are classified by their mass. For example, the masses of Class* 1 UAS are less than 150 kg and Class 2 UAS masses are between 150 and 200 kg. It is convenient to further subdivide Class 1 UAS as shown in the following table.

*L-3 Communications ASA Ltd, Rusint House, Harvest Crescent, Fleet, Hampshire, GU51 2QS, UK
email: paul.easthope@L3T.com
†L-3 Communications ASA Ltd, Rusint House, Harvest Crescent, Fleet, Hampshire, GU51 2QS, UK
email: alancollinson@compuserve.com

*The classification system was developed, *inter alia*, by the US Army.

| *Class* | *Mass* |
|---|---|
| Nano | $< 500$ g |
| Micro | 500 g to 2 kg |
| Mini-light | 2 kg to 10 kg |
| Mini-heavy | 10 kg to 20 kg |
| Macro | 20 kg to $< 150$ kg |

The work described below is principally concerned with UAS of less than 10 kg (mini-light), and the factors relating to this choice are discussed below.

Even the smallest of these classes of UAS can carry a camera and may retail for less than US$200. It is possible to purchase a nano UAS, carrying a 14 Mpixel camera and capable of flying for 20 minutes, for less than US$700. (Whereas, mini-heavy UAS airframes might cost US$60,000). Nano and micro classes of UAS might be expected to be under manned control for their whole flight, and an alternative name for UAS is Remotely Piloted Air Systems (RPAS). If the UAS carries a camera and video can be relayed in real-time, then the pilot need not have direct line of sight to the target. The smallest and cheapest UAS maximum flight time may be less than 5 minutes, but for the slightly more expensive nano and micro UAS, flight times of 20 to 30 minutes are more typical. Ranges may be as low as 2 km, determined by the range of the radio control. Altitudes will usually be less than 1,000 feet and airspeeds of the order of tens of metres per second ([2]).

By comparison, mini-heavy UAS may be under manual control for their whole flight but may also incorporate a degree of autonomy. For example, it may be possible to instruct them to fly autonomously to a desired location via waypoints, using the Global Positioning System (GPS) or alternatives to navigate. The mission endurance is high, perhaps as much as 20 hours, and a maximum range of 100 km might be achieved with a cruising speed of 20 $\text{ms}^{-1}$ and a maximum speed of 30 $\text{ms}^{-1}$. Operating altitudes could be 15,000 feet or higher. With this size of vehicle, a wider range of payload options is available and these payloads might be powered by an onboard generator ([3]). This class of UAS is larger and more readily detectable than smaller classes.

UAS may also be classified by airframe and method of motive power which includes: fixed wing, rotary wing, rocket-powered and hybrid. It will become clear from examining this list that UAS can have a wide range of flight dynamics and may even be capable of changing dynamics in flight. For example, rotary wing UAS are capable of stopping flying, perching, and then returning the powered flight during a sortie. The different sub-categories lend themselves to different missions and multiple independent UAS may be present in the battlefield at any one time ([10]).

The smaller classes of UAS are physically small and have low acoustic, optical, infrared and radar signatures. The flight characteristics and piloting options can readily facilitate screening of the UAS from sensors using either terrain or the built environment; indeed, environments such as urban canyons may be particularly challenging

There are a number of reasons why it may be desirable for an adversary to use a swarm of UAS:

- To spread the mass of the mission functionality across a number of different platforms.

For example, one or more UAS may collect reconnaissance information, while other UAS in the swarm may share responsibility for air-to-ground and ground-to-air communications.
- To increase the weapons load and/or the variety of weapons.
- To make the attack more robust (*i.e.* less susceptible to the attack failing if some platforms are negated).
- To make a deliberate show of strength.
- And, while there are many others, perhaps the most significant reasons are to saturate, out-flank or out-manœuvre defences.

Equally important as the reasons for using a swarm is the fact that swarms are now affordable. Furthermore, even when the cost of an attack is multiplied by the number of UAS in a swarm, extremely high exchange ratios might be possible.

There does not appear to be a universally accepted definition of the numbers of UAS that constitute a swarm. Most dictionary definitions of 'swarm' simply refer to 'large numbers'. One factor that might limit numbers in a swarm is the ability to control many UAS at one time, although greater degrees of autonomy mitigate the control problem. The US Office of Naval Research (ONR) has already demonstrated the ability to launch and recover 30 UAS at one time ([1]) while Intel, in conjunction with Ars Electronica Futurelab, demonstrated in November 2015 the ability to control 100 UAS concurrently in a performance artwork, requiring a high degree of control ([4]).

The presence of potentially large numbers of UAS in a sensor field of regard concurrently places many challenges on the defence, which may be listed as follows:

- Detection and transition to track:
  - UAS of interest have small size and may be built using composite materials, giving rise to small signatures.
  - UAS operators may exploit natural and man-made screening to reduce viewing opportunities.
  - UAS may be eclipsed in flight by other UAS.
- Track maintenance:
  - Multiple, and changing, flight dynamics.
  - UAS may fly in close formation with degraded radar resolution.
- Classification and identification:
  - Determining a reliable head count (the number of UAS).
  - Detecting changes in head count.
  - Assessing intent and detecting feints.

  - If functionality is spread across the swarm, collateral information from Electronic Support Measures (ESM) may be limited to only a subset of the swam members.

- Decision support challenges:

  - Short ranges to target can limit the decision-making space.

The overriding challenge is to perform all of the above and leave time to sentence (decide if the swarm is to be engaged and how), and then to negate the threat. For the purposes of the present paper, however, the work described here concentrates upon developing a viable tracking solution in the situation where a UAS swarm is manœuvring in a more or less coherent manner.

In view of the foregoing discussion, it is evident that attempting to track UAS swarms using a radar (or a network of distributed radars) presents severe challenges. For the above-stated reasons, individual UAS may be seen perhaps only once every several sensor looks, and if this is combined with quasi-random UAS dynamics, it can be appreciated that a conventional point-target tracking system is likely to produce only sequences of short-lived and erratic tracks, from which the swarm size and intent may be difficult or impossible to discern.

The approach taken here, as in [6], is to admit that it may not be possible to track each individual UAS, but that it is nonetheless valuable to be able to extract a stable trajectory for the swarm as a whole and — where possible — to be able to infer the numbers of UAS present and their spatial dispersion.

Section 3 provides a brief description of an algorithm capable of simulating simple swarm behaviour, so far as it is at present understood, while Section 4 defines the tracking filter logic. The tracking results are summarised in Section 5.

## 3. SWARM SIMULATION

An earlier paper [6] has already described an algorithm that can simulate at least some characteristic elements of swarm behaviour. The same logic is used here, and the main elements are summarised as follows:

The swarm as a whole comprises ten members and is assigned a definite base trajectory to follow (a deliberately variable, near-random, path is used in the example below). Each UAS within the swarm is then envisaged to be aware of the distance to all of its neighbours*; the individual UAS dynamics are then governed by a linear combination of accelerations toward or away from neighbours, using an attractive force for more distant ones but a repulsive one for nearer ones. In addition, the resultant UAS velocity is formed from a weighted linear combination of its own velocity and that of the swarm as a whole, with a superimposed randomness to emulate environmental effects such as wind gusts. The net effect is that the swarm follows its assigned trajectory with some fidelity, while the individual UAS have rather more wandering paths relative to the swarm centroid. The nature of the simulation algorithm means that there is no one consistent leader. A more or less constant altitude of 500 m is maintained and an average speed for the swarm of 20 $\mathrm{ms}^{-1}$.

*This can be restricted to those 'ahead' of it, thus emulating forward vision only.

Figure 1 shows a top-down view of the swarm trajectory, spanning 1900 s, with motion at top-left and moving downward. The constituents are initially bunched fairly close together, with separations typically of the order of 100 m or less, and the individual trajectories tend to slowly diverge over time.

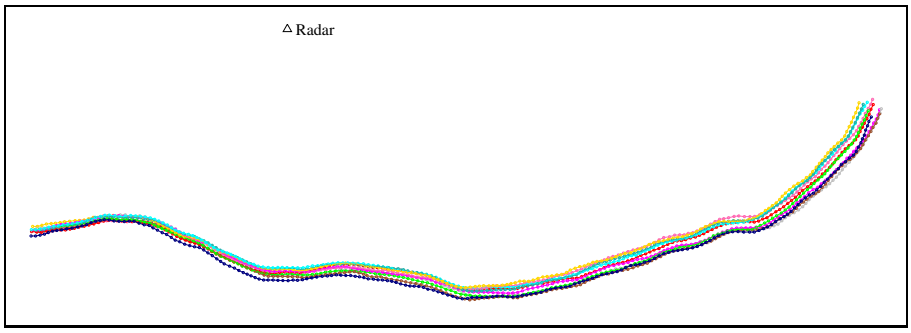


Fig. 1. Underlying UAS constituent trajectories

Each individual UAS is assigned a different colour and it can be seen that their trajectories move toward and away from each other, interleave and so forth; this is deliberately not intended to be 'formation flying'.

Simulated radar measurements are then provided by the single sensor marked on Figure 1, located at about 9 km from the trajectory at its closest point, giving normally-distributed polar range, azimuth and elevation measurements at a rate of 0.1 Hz. The range uncertainty was fixed at 30 m and the angular uncertainty at 2.2 mrad, thus enabling target resolution in range (swarm configuration permitting) but typically not resolution in angle.

This radar is assumed to provide whatever individual returns it can obtain on the individual swarm constituents — there is no attempt to collapse sets of returns at the same time into a centroid and uncertainty representing that group. The tracking system in Section 4 is thus intended to work with 'unclumped' returns.

To emulate radar sensitivity, each swarm member is assumed to have a mean Radar Cross Section of 0.01 $m^2$ under Swerling 1 statistics and with a noise floor of 10 dB imposed on the Signal to Noise Ratio (SNR). Thus, as the range increases, measurements on individual swarm members become sparser and as a consequence the number of swarm members seen per look diminishes. At the beginning of the scenario, individual target probabilities of detection are typically above 0.9, whereas toward the end of the scenario the values are nearer to 0.5 (although in both cases with considerable variation across the target set). Clutter has not been simulated.

A short section of radar plots spanning about 170 s near the centre of Figure 1 is shown in Figure 2, using a top-down view. Plot uncertainty is represented by an ellipse, although the uncertainty axes are approximately the same at this sensor-target range of 12 km.

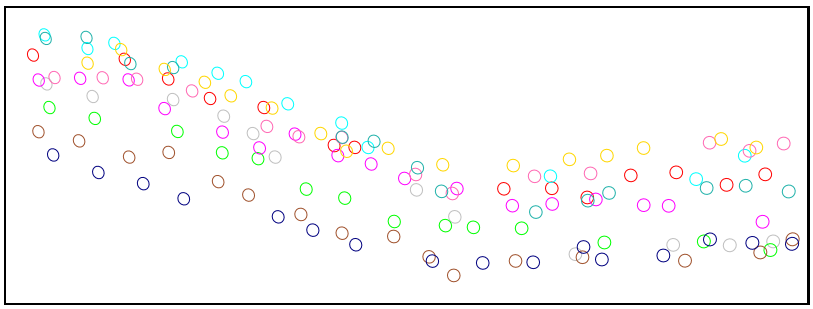

Fig. 2. Section of radar measurements at about 12 km from the radar

Again, the colour-coding reflects the UAS identity. This is quite near to the radar, so there are few missing observations (in contrast to later sections of the scenario). Even though individual trajectories can be visually identified, it can be appreciated that tracking each constituent is complicated by their close spacing and irregular motion.

In contrast, Figure 3 shows a longer time segment of plots spanning 420 s at the end of the trajectory, at about 22 km from the radar.

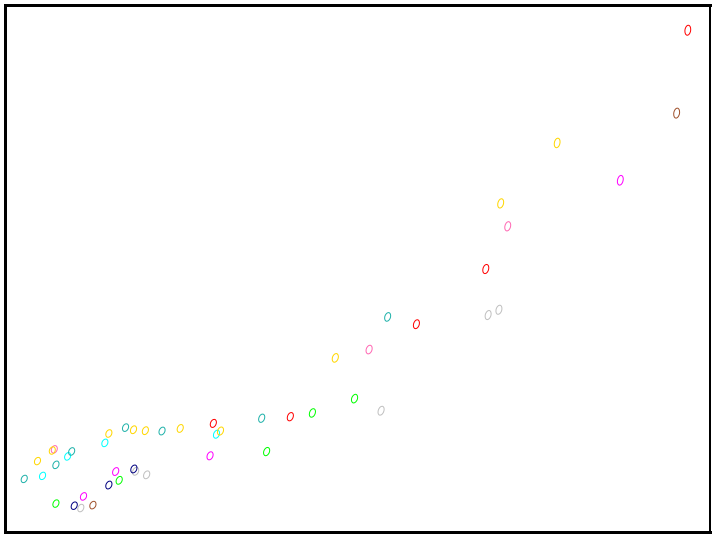

Fig. 3. Section of radar measurements toward trajectory end

In this case, missing observations give rise to a much more challenging tracking environment and it can be appreciated that the problems will be exacerbated in the presence of even more swarm members than the ten used here.

## 4. TRACKING LOGIC

Tracking the measurements on the UAS swarm described in Section 3 with a point-target tracker results in numerous disconnected track fragments, with any longer-lived ones exhibit-

ing significant levels of miscorrelation. Apart from a brief interval toward the start, nearest to the radar, it would be difficult to discern swarm intent, or to gain an estimate of the number of constituents.

Reference [6] described a tracking solution for the swarm centroid and dispersion using particle filter concepts, which seemed a natural fit to the task in hand. However, the resulting filter proved to be more complex than is desirable, largely due to the need to maintain particle density under conditions of less than perfect conditions. In contrast, in the present case, a much simpler Kalman-based filter has proved adequately robust, as well as being able to support threat count analyses, for example.

The basic concept assumes that the main requirement is to be able to maintain a stable track on the swarm centroid, despite being given quasi-random radar observations dispersed relative to that centroid. Thus, as a baseline, a Cartesian Earth-Centred Inertial (ECI) constant-velocity model (see, for example, [5]) is defined in three-dimensional space, giving a 6-dimensional basic state vector*. Three further state vector components are then added, representing measurement offsets in range and angle relative to the centroid.

It should be noted that no attempt is made to pre-process each scan of radar data into a centroid plus dispersion prior to tracking; the aim is to supply the tracking filter with radar returns from the individual UAS as they occur in time. The filter itself estimates centroid and dispersion simultaneously.

In index form, the kinematic equations are as follows, with a superscript dot standing for time derivative:

$$\ddot{x}_i = \nu_i, \quad \text{for } i = 1, 2, 3, \tag{1}$$

$$\dot{\zeta}_j = -\alpha\zeta_j + w_j, \quad \text{for } j = 1, 2, 3. \tag{2}$$

Here, $x_1$, $x_2$, $x_3$ stand for the ECI $x$, $y$, $z$ position components respectively, while the $\zeta_1$, $\zeta_2$, $\zeta_3$ states represent measurement offsets from the track position in the range and angle directions respectively; these are assumed to evolve in time according to a first-order Markov process with fixed parameter $\alpha$. For present purposes, $\alpha = 0.2$; although it is known that $\alpha > 0$ is required for filter stability, its actual value does not appear to be critical.

Thus, the nine state vector components are $[x_1,\ x_2,\ x_3,\ \dot{x}_1,\ \dot{x}_2,\ \dot{x}_3,\ \zeta_1,\ \zeta_2,\ \zeta_3]$ and the quantities $\nu_i$ and $w_j$ stand for process noise.

The $\zeta_i$ state components relate to the polar radar measurements according to the measurement equations

$$z_k = h_k(x_i) + \zeta_j + v_k, \tag{3}$$

where $h(.)$ stands for the measurement function converting from Cartesian ECI into polar coordinates relative to the sensor position, $v_k$ is measurement noise and the $x_i$ span the state position components only. Thus, for example, if $\zeta_1$ is the tracked range offset relative to the swarm centroid, then the sensor-target range $\lambda$ relates to the $x_i$ as follows:

$$\lambda = \sqrt{(x - r_x)^2 + (y - r_y)^2 + (z - r_z)^2} + \zeta_1 + v_\lambda, \tag{4}$$

and where the $r_x$, *etc*, denote the ECI sensor location components.

*Three components each of position and velocity.

With regards to the process noise levels, $\nu_i = 0.05$ ms$^{-2}$ works well, while the individual $w_j$ need to be set according to the measured or expected UAS dispersion in the relevant measurement dimension. It has also been found advantageous to adapt the angular process noise magnitudes according to the perceived swarm dispersion, which may change slowly over time; the time-averaged weighted distance measure provides a means to do this, and the logic is described in Appendix B.

Track initiation uses the first two asynchronous radar measurements in the usual manner and each subsequent measurement is subject to a gating criterion, using a fixed gate value of slightly over 99%.

Experience has shown that the formulation of equation (2) ensures prompt responsiveness to oscillatory or abrupt random variations in the offsets, behaviour which is well-suited to the present requirements, in which each measurement is likely to appear completely uncorrelated with its predecessor in time.

The constant-velocity model was chosen largely because this imposes the most constraint upon track velocities. The constant-acceleration model or the Singer model (both of which are described in [5]) provide valid general-purpose alternatives, but their less restrained motions tend to cross-feed into the offset states. The more constrained the centroid tracking model, the more accurately will the offset states reflect the actual swarm dispersion.

The above tracking model is, as is shown in the next section, capable of tracking the swarm centroid and inferring the dispersion of the individual UAS simultaneously. A brief discussion of system observability is provided in Appendix A and sample tracking results are examined in Section 5.

The response of the above filter to clutter has yet to be assessed. It can be anticipated that low levels of environmental clutter will merely perturb an existing swarm track, or initiate a new one if the clutter return is outside the swarm gates. Heavy clutter may well prove detrimental, although further work is needed to explore its actual effects.

## 5. TRACKING RESULTS

The resulting track on the UAS centroid is shown in Figure 4, here colouring by track identity number and with the centroid spatial uncertainties denoted by ellipses.

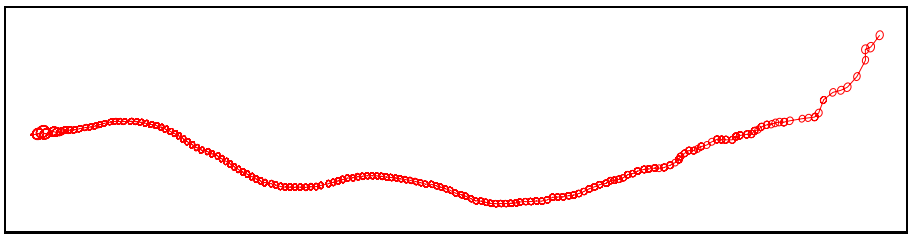

Fig. 4. Track on UAS centroid

It is evident that despite the irregular overall swarm trajectory and the independent motion of the constituents, it is possible to track the centroid continuously — even toward the end, when the measurements are much sparser. Quite stable velocity components can also be extracted, as shown in Figure 5.

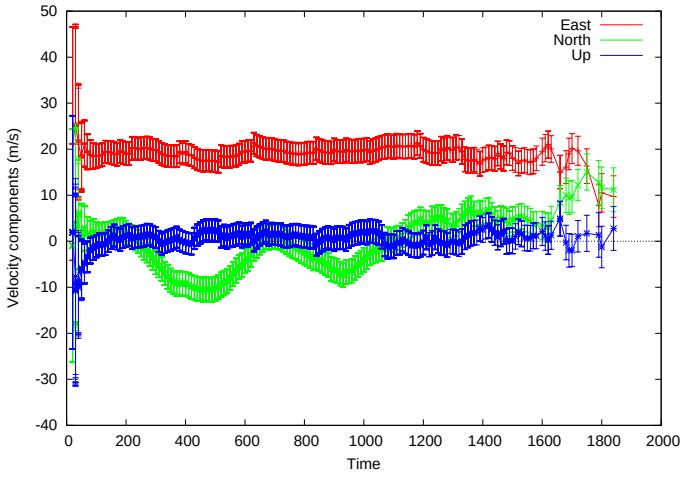


Fig. 5. East, north and up centroid velocity components

The error bars indicate the associated velocity component uncertainty and it can be seen that the swarm is maintaining a more or less stable altitude, as intended. The effects of the measurement sparsity can also be discerned at the end of the trajectory.

Also of interest is the behaviour of the state offset $\zeta$-components, which are shown in Figure 6.

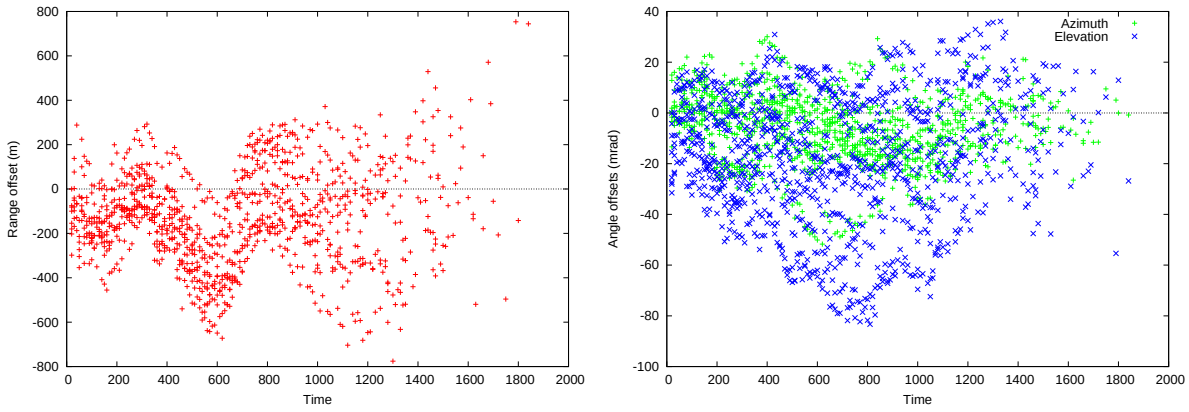


Range Angle

Fig. 6. Tracked range and angle $\zeta$ offsets

These give some indication of the swarm dispersion relative to the radar, and also clearly show the effects of decreasing individual UAS visibility as the swarm moves away from the sensor. Although it is not easy from Figure 6 to discern the number of constituent UAS present, there are patterns in the data which can be seen more clearly over a shorter time

period and when colouring and joining by UAS identity. The results are shown in Figures 7 and 8.

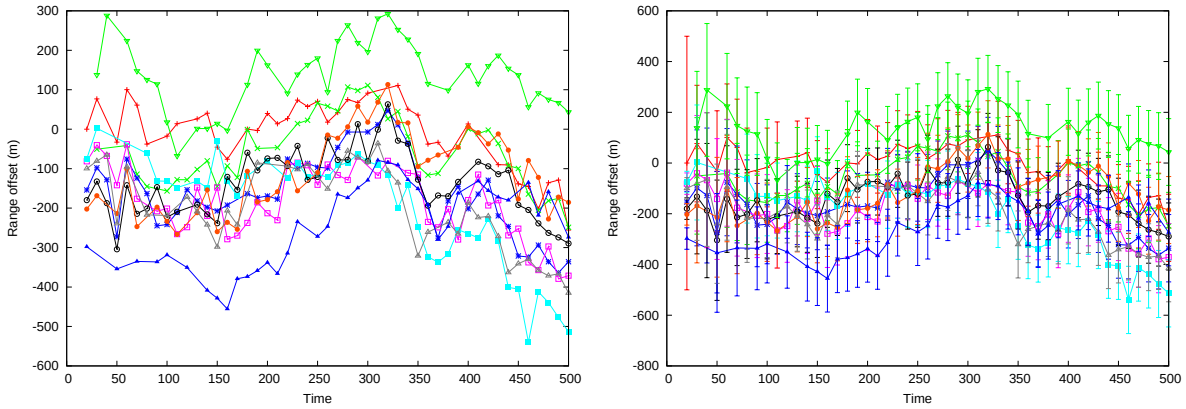


Range Range (with uncertainties)

Fig. 7. Tracked range $\zeta$ offsets, colouring by UAS identity (detail)

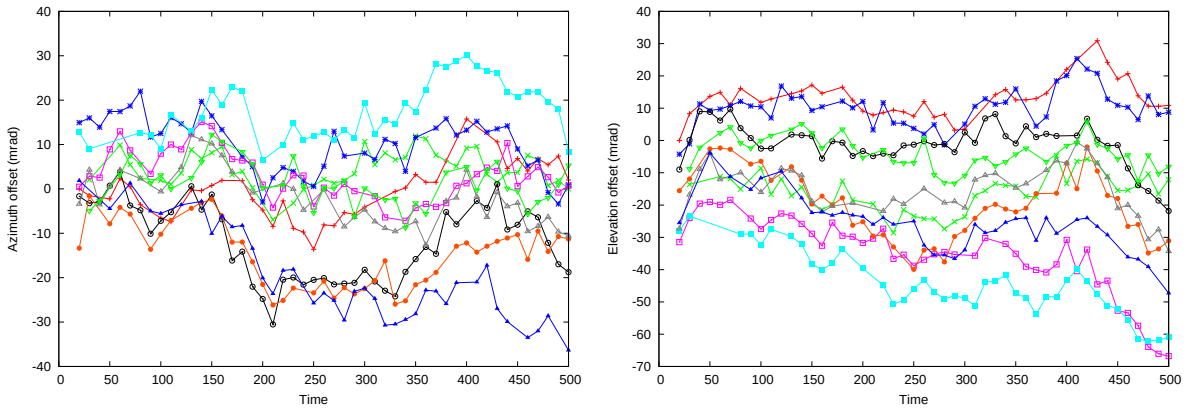


Azimuth Elevation

Fig. 8. Tracked angle $\zeta$ offsets, colouring by UAS identity (detail)

The second range offset plot contains the associated one-sigma $\zeta$-uncertainties, showing the considerable degree of overlap across the target set*. It is not obvious that the data as shown could be further processed to reveal the threat count. A more certain tracking model (necessarily dependent on predictable swarm motion) or a more rapid radar revisit rate might enable such processing to take place, as would more accurate range measurements. Indeed, the latter capability combined with the above offset tracking may permit the reconstruction of

*Similar comments apply to the azimuth and elevation offset data sequences.

individual UAS trajectories even in the complete absence of any angular resolution. This is in contrast to the more familiar Kalman Filter behaviour in which range and angle uncertainties tend to cross-feed, typically to the benefit of the latter and the detriment of the former.

In the present case, with regard to threat count, the method proposed in [6] — namely, to count the number of measurements seen per radar 'look' — can be applied here, giving Figure 9.

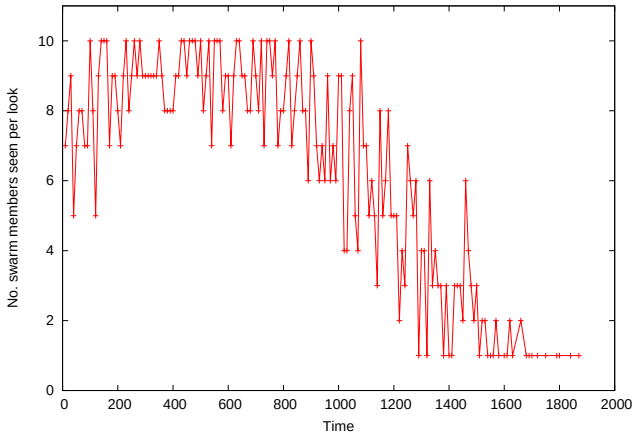


Fig. 9. Count of measurements per radar 'look'

For about the first 1000 s or so, it can be inferred from the 'ceiling' values found over time that the swarm contains ten constituents. Thereafter, decreasing target observability degrades the threat count estimates.

The final point of interest concerns a visual estimate of the swarm spatial extent, which can be obtained by processing the $\zeta$-offsets into ECR coordinates and creating something akin to an uncertainty (or dispersion) ellipse. The results are shown in Figure 10.

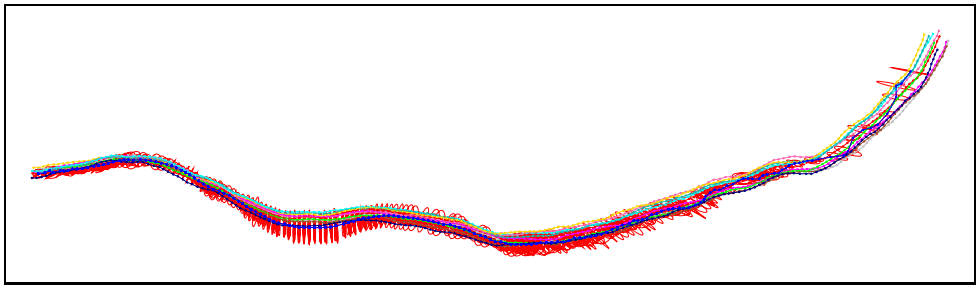

Fig. 10. Tracked swarm dispersion, with superimposed truth trajectories

Here, the individual UAS trajectories are denoted by the thin multi-coloured lines, while the dispersion ellipses are coloured red. The irregular thin blue line marks the track centroid over time. It can be seen that the dispersion matrices give a reasonable estimate of the swarm

spatial extent, although there is some evidence that the centroid is slightly slow in responding to swarm changes of course. This can be corrected by increasing the process noise levels*, although to the detriment of the centroid position and velocity estimates.

## 6. DISCUSSION

It was assumed at the commencement of the present work that swarms of UAS are now realisable at low cost and that the ability to track such swarms will become a necessary part of any surveillance or defensive measures. It was also assumed that swarm members will obey two basic rules:

1. Avoid collisions with other swarm members,
2. Not become completely detached from the swarm as a whole.

Using currently-available knowledge of the characteristics of speed, altitude and observability of UAS, a quasi-random model of swarm behaviour was developed and reported in [6]. That same work also described a particle filter suitable for tracking the swarm.

That work has now been extended to examine whether it is possible to track the swarm using simpler linear Kalman Filters. Thus, in the present case, the familiar constant-velocity model follows the swarm centroid, while additional track states respond to the individual UAS offsets in range and angle relative to that centroid. This tracking model is simpler than the particle filter proposed in [6] and satisfies the following requirements:

- The position and velocity of the swarm centroid can be tracked, probably sufficiently well to cue an optical sensor (although this remains to be demonstrated).
- Some indication of the swarm extent can be gained from the additional track states.
- An estimate of number of members in the swarm is obtainable indirectly from the numbers of measurements achieved per time period.

For the future, it is anticipated that both friendly and unfriendly swarms of UAS and other types of air platforms will be present concurrently in the sensors field of regard. It is foreseen that the ability to track swarms will facilitate other data fusion activities of picture compilation and Threat Evaluation and Sensor and Weapon Allocation (TESWA).

It is also worth mentioning that the same form of tracking model (containing highly responsive offset states) works well in similar contexts where, for whatever reason, point-target tracking the individual constituents in a cluster becomes difficult or impossible. Such situations include tracking in the presence of large radar glint errors, or where numerous small objects have been deployed from a satellite or ballistic missile and thereafter diverge slowly over time. The more accurately the tracking model can be specified, the better the stability and representativeness of the offset components, so the technique is not considered suitable in the presence of abrupt manœuvres or imperfectly-known dynamics.

Future work in this area should involve a more detailed examination of how a UAS swarm actually appears to a radar, preferably incorporating real data. It is also necessary to assess how the above tracking model responds to clutter, swarm merging, constituent dispersal and other real-world phenomena (such as clutter and terrain screening). Alternative swarm simulation algorithms would also be of interest, but an examination of the open literature in this context has yet to be carried out.

*Or by adopting a constant acceleration, rather than constant velocity, model.

## ACKNOWLEDGEMENTS

This work has been supported in entirety by L-3 Communications ASA Ltd.

## REFERENCES

[1] 'Locust' swarm experiments: http://www.onr.navy.mil/media-center/press-releases/2015/locust-low-cost-uav-swarm-onr.aspx. Accessed 11 july 2016, Office of Naval Research, USA, 14 April 2015.

[2] *AeroVironment UAS*. AeroVironment, USA, https://www.avinc.com/uas/adc/black_widow, Accessed 11 July 2016.

[3] *UAV Factory*. UAV Factory, USA, http://www.uavfactory.com/page/technical-data, Accessed 11 July 2016.

[4] *FutureLab*. Ars Electronica, https://www.aet.at/futurelab/en/project/drone-100, Accessed 26 September 2017.

[5] S. Blackman and R. Popoli. *Design and Analysis of Modern Tracking Systems*. Artech House, Norwood, 3 edition, 1999.

[6] P. Easthope. Tracking simulated UAV swarms using particle filters. In *Proceedings of the 10th IET Data Fusion and Target Tracking Conference*, UK, 2014. University of Liverpool.

[7] A. Gelb. *Applied Optimal Estimation.* MIT Press, Cambridge, 1974.

[8] T. Glad. Dynamic systems: Lecture 2 — observability. reglerteknik. ISY, Linköpings Universitet, 2014.

[9] J. Hedrick and A. Girard. *Control of Nonlinear Dynamic Systems: Theory and Applications*. Printed Course, Universita Degli Studi di Padova, 2005.

[10] P. Karber. Lessons learned from the Russo-Ukrainian war: Personal observations. Technical report, The Potomac Foundation, 2015.

[11] L. Klein. *Sensor and Data Fusion: A Tool for Information Assessment and Decision Making*. SPIE Press, 2004.

[12] G. Sartoretti, M.-O. Hongler, M. de Oliveira, and F. Mondrada. Decentralized self-selection of swarm trajectories: from dynamical systems theory to robotic implementation. *Swarm Intelligence*, 8(4):329–351, 2014.

## A. OBSERVABILITY

For the purposes of examining the system observability, and the observability of the offset $\zeta$ states in particular, it is convenient to simplify the tracking model to a locally flat Cartesian system. In addition, the sensor will be placed at the origin, although retaining polar measurements in range, azimuth and elevation. That is, the state vector is as follows:

$$[x,\, y,\, z,\, u,\, v,\, w,\, L,\, \psi,\, \eta] \equiv x_k \quad \text{for } k = 1, \ldots, 9,$$

the final three being the offset components, and with the associated kinematic model:

$$\begin{aligned}
&\dot{x} = u, \quad \dot{y} = v, \quad \dot{z} = w,\\
&\dot{u} = 0, \quad \dot{v} = 0, \quad \dot{w} = 0,\\
&\dot{L} = -\alpha L, \quad \dot{\psi} = -\beta\psi, \quad \dot{\eta} = -\gamma\eta,
\end{aligned}$$

where a superscript dot implies time derivative and ignoring process noise for the observability assessment. The parameters $\alpha$, $\beta$, $\gamma$ are assumed fixed and not necessarily equal.

A sequence of range and angle measurements are assumed available, with range $\lambda$ and polar angles $\phi$ and $\theta$ relating to the state components as follows:

$$\begin{aligned}
\lambda &= \sqrt{x^2 + y^2 + z^2} + L, \\
\phi &= \tan^{-1}\left(\frac{y}{x}\right) + \psi, \\
\theta &= \sin^{-1}\left(\frac{z}{\sqrt{x^2 + y^2 + z^2}}\right) + \eta.
\end{aligned}$$

Since this is a nonlinear kinematic system, the familiar linear observability matrix $\Xi$ relating a discrete sequence of measurements to the state components (see [7]) is inapplicable. Rather, recourse can be made to the Lie derivative approach ([8] and [9]), in which observability is assessed in terms of successive derivatives of the measurement components.

That is, the question is asked, given $\lambda$, $\phi$, $\theta$ and successive derivatives thereof, can one determine all of the state components — and the offset states in particular — from the above measurement and state equations?

It is not difficult to show that $L$ is globally observable, since if the definition $R(x, y, z) = \sqrt{x^2 + y^2 + z^2}$ is made, then the following differential equation follows:

$$R\frac{d^3R}{dt^3} + 3\frac{dR}{dt}\frac{d^2R}{dt^2} = 0.$$

Since $R = \lambda - L$ and the various derivatives of $\lambda$ are assumed known, a quadratic equation in $L$ results, which can be solved (at least in principle).

With regards to the angle offsets $\psi$ and $\eta$, however, the situation is more complex, resulting in transcendental equations with no obvious (let alone straightforward) solutions. Thus, it has been necessary to revert to an examination of *local* observability ([8], [9]), with logic as follows:

Define the column vector

$$\begin{aligned}
\underline{g} &= \left[\lambda,\, \phi,\, \theta,\, \dot{\lambda},\, \dot{\phi},\, \dot{\theta},\, \ddot{\lambda},\, \ddot{\phi},\, \ddot{\theta}\right] \\
&\equiv g_j, \quad \text{for } j = 1, \ldots, 9.
\end{aligned}$$

Then, if the $9 \times 9$ matrix

$$\partial G \equiv \frac{\partial g_j}{\partial x_k}$$

is of rank 9, where $x_k$ is defined above, the system is locally observable.

Leaving aside the algebra, the components of vector $\underline{g}$ are found to be:

$$
\begin{aligned}
g_1 &= R + L, \\
g_2 &= \tan^{-1}\left(\frac{y}{x}\right) + \psi, \\
g_3 &= \sin^{-1}\left(\frac{z}{R}\right) + \eta, \\
g_4 &= \frac{C}{R} - \alpha L, \\
g_5 &= \frac{(xv - yu)}{(x^2 + y^2)} - \beta\psi, \\
g_6 &= \frac{1}{\sqrt{x^2 + y^2}}\left[w - \frac{z\,C}{R^2}\right] - \gamma\eta, \\
g_7 &= \frac{V^2}{R} - \frac{C^2}{R^3} + \alpha^2 L, \\
g_8 &= -2\frac{(xv - yu)\,(xu + yv)}{(x^2 + y^2)^2} + \beta^2\psi, \\
g_9 &= -\frac{(xu + yv)}{(x^2 + y^2)^{3/2}}\left[w - \frac{z\,C}{R^2}\right] + \frac{1}{R^2}\frac{1}{\sqrt{x^2 + y^2}}\left[-Cw - zV^2 + \frac{2zC^2}{R^2}\right] + \gamma^2\eta,
\end{aligned}
$$

where

$$
R = \sqrt{x^2 + y^2 + z^2}, \quad V = \sqrt{u^2 + v^2 + w^2}, \quad \text{and} \quad C = xu + yv + zw
$$

have been defined for convenience.

Carrying out the relevant partial derivatives of $g_j$ with respect to $x_k$ — a task devolved to the Maple™ symbolic manipulation package — results in a partially-populated matrix $\partial G$ (for brevity, the lengthy elements of this matrix are not explicitly listed here). It is then possible to make use of the `rank()` command within Maple™ to show that $\mathrm{rank}(\partial G) = 9$. It may be concluded that the system is at least locally observable in the manner defined in [8] and [9].

## B. ADAPTIVE PROCESS NOISE

It was mentioned in Section 4 that more robust tracking is obtained if the process noise values for the two angular offset states $\zeta_2$ and $\zeta_3$ are made responsive to the perceived swarm extent, and the logic for this is described below. A single fixed uncertainty value for the range offset $\zeta_1$ was found to be adequate.

Let the angular process noise magnitude be denoted by $w$, let $d^2$ stand for the weighted distance measure (also known as the Mahalanobis distance [11]) and $\overline{d^2}$ for its recursively-averaged value. The following sequence of operations is then applied:

- Retain the process noise $w$ from update to update according to the recursive equation

$$
w \rightarrow Gw + (1 - G)\, w_{min}, \tag{5}
$$

where $G$ is a gain factor and $w_{min}$ represents a suitable lower bound (set to $10^{-5}$ rad by default).

- The gain factor $G$ is set equal to the larger of a fixed value $G_{min}$ and $1 - \Delta t(1 - \overline{d^2})$, where $\Delta t$ is the time step. The use of a lower bound on $G$ prevents the retained process noise from diminishing too rapidly.

  Note that if $\Delta t = 0$, the gain is automatically set at unity, retaining the process noise unchanged.
- The values of $w$ are bounded above by 5 mrad (by default), to prevent divergence.

The logic behind equation (5) is based on the assumption that, for a stable swarm size, the uncertainty of the additional track states $\zeta_j$ should decay with time $t$ according to the generic formula

$$w(t) = w_{min} + p\, e^{-\mu(t-t_0)},$$

for constant $p$ and rate of decay $\mu$. The decay factor $\mu$ is then made dependent on $1 - \overline{d^2}$, so that $\overline{d^2} > 1$ gives rise to increased process noise, while $\overline{d^2} < 1$ permits it to decay.

Note that the actual weighted distance measure $d^2$ is a random quantity with expected mean equal to the number of measurement degrees of freedom, $m$ (3 for a radar, 2 for a passive sensor and so forth). To allow for mixes of sensor types, $\overline{d^2}$ was defined as

$$\overline{d^2} = \frac{1}{N} \sum_{1}^{N} \frac{d_i^2}{m},$$

where $N$ is a measurement counter. This is independent of the number of degrees of freedom and can be written in recursive form:

$$\overline{d^2}_k = (1 - \eta)\overline{d^2}_{k-1} + \eta \frac{d_k^2}{m},$$

for update $k$ and where $\eta$ is the larger of $1/k$ and $1/200$ (to provide some responsiveness to new information).

The feedback-type mechanism described here provides a balance between responsiveness and robustness. It is unlikely to be the only solution but various modifications that were attempted invariably proved detrimental.

ABSTRACT

The proliferation of cheap Unmanned Aerial Systems (UAS) poses some significant challenges for the Ground Based Air Defence (GBAD) environment. Individual UAS are inherently difficult to detect, track, classify and identify, but the challenges are exacerbated if UAS are deployed in swarms. It can be appreciated that small physical size, combined with the extensive use of non-metallic materials, will render an individual UAS difficult to detect from a radar's perspective. If such targets are deployed in a group, then the radar response is likely to consist of intermittent, uncorrelated observations on random subsets of the swarm as a whole, with no guarantee that observations made on individual constituent UAS will be consistent from scan to scan.

This paper describes a tracking filter model that is able to simultaneously track the swarm centroid and the spatial dispersion of constituent UAS, without requiring any pre-processing of radar returns into clusters.

Although this paper is primarily concerned with UAS, the authors are aware that other types of platform may usefully be employed in swarms, for example satellites, and that some large and complex unitary systems may present swarm-like characteristics to sensors. The principles discussed here may also be applicable in these other cases.

## ŚLEDZENIE ROJÓW BEZZAŁOGOWYCH STATKÓW POWIETRZNYCH

Paul F. Easthope, A. Collinson

W artykule zamieszczono równania określające oczekiwane liczby linii przechodzących przez $k$ punktów, zdefiniowanych jako wąskie prostokątne obszary o zadanych wymiarach, które można znaleźć w szerszym kwadratowym obszarze zawierające punkty rozmieszczone z rozkładem normalnym. Zamieszczono wyniki symulacyjne, stanowiące podstawę do oceny prawdopodobieństwa tego, że liniowe serie pomiarów w środowisku zakłóconym mają charakter losowy.

Received: 2018-02-13
Accepted: 2018-04-16